FOI
SWEDISH DEFENCE
RESEARCH AGENCY

FOI-R--0370--SE
January 2002
ISSN 1650-1942
Methodology report

Dynamical Detection of Hydroacoustic Signals Recorded at a Sea Trial in the Baltic Sea

Ron K. Lennartsson

Systems Technology
SE-172 90 Stockholm

Contents

1 Introduction

In this report we present a detection study on real-world sonar recordings using a deterministic time domain method. Specifically, we discuss the estimation of the parameters of a nonlinear delay differential equation from this data. Using these estimated model coefficients as detection features we design signal detectors by implementing a Mahalanobis distance-based decision criteria to perform rigorous hypothesis testing and characterize performance. By analyzing acoustic data recorded in shallow water in the Baltic Sea, we compare the performance of the dynamical detector with a frequency band-matched energy detector and demonstrate that the former provides increased detection performance. Since the dynamical detector does not include signal information due to energy fluctuations, we also construct a hybrid detector which incorporates dynamical and energy features, and compare this performance to the simple energy detector.

In general dynamical detectors should be sensitive to signal structure which is generated by low-dimensional dynamics from some physical system. Hence, we expect that they should provide good performance on signals derived from e.g. mechanical systems. They also can provide more parsimonious representations of such data than spectral methods, hence we hypothesize that the dynamical detectors may be very useful for signals which are deterministic but moderately broadband. As the boat signatures discussed here are already known to possess some nonlinear structure by previous analyses using bispectral methods, the intention of this study is to characterize the performance on such signatures using the dynamical methods.

2 Estimation of Nonlinear Dynamical Models

Here we present a brief description of our model estimation procedure using time-domain delay differential equation signal models. For a detailed description the reader is referred to [1, 2]. Delay differential equations are utilized due to generality of their solution spaces, and their generally easier treatment over ODEs in the context of the dynamical model estimation problem. Coefficients estimated by this procedure are then used as features in the detection process, which will be discussed in the next section.

We first assume that we observe a continuous scalar data stream $x(t)$ generated by a measurement of some physical process. We hypothesize that the process evolution itself can be reasonably approximated by a deterministic, relatively low-dimensional dynamics. Using up to D time-delayed copies of $x(t)$, written $x(t-\tau_d)$ with $1 \leq d \leq D$, and introducing the shorthand notation $x \equiv x(t)$,

$\dot{x} \equiv \dot{x}(t)$, and $x_\tau \equiv x(t-\tau)$, our general model form is:

$$\dot{x} = F\left(x, x_{\tau_1}, \ldots, x_{\tau_D}\right). \tag{1}$$

The function F is often expanded in terms of some basis functions. For our analysis here we will restrict our attention to a two-delay second order model of type

$$\dot{x} = a_1 x_{\tau_1} + a_2 x_{\tau_2} + a_3 x_{\tau_1} x_{\tau_2}. \tag{2}$$

Equation (2) has been used successfully to model and detect deterministic quadratic phase couplings [1], for example.

Our goal here is not to create an exact model for the signal but rather to find a relatively few dimensional (small D) and low order (preferably quadratic or cubic) model form, which allows us to distinguish between the signal classes of interest. By defining a general model representing several signal classes the model is in fact used as a fixed "dynamical filter" which allows direct comparison between the various signal classes.

The model coefficients a_1, a_2, and a_3 in Eq. (2) are estimated for each data window, and they comprise our classification feature space. This estimation must be numerically robust and preferably preserve the low-order nonlinear correlations that might be present in the original signal. Here we present a method which can accomplish both of these goals, and make explicit connection to higher-order spectral theory [1][3]. To proceed, we multiply Eq. (2) consecutively by each basis term x_{τ_1}, x_{τ_2}, and $x_{\tau_1} x_{\tau_2}$ to generate a system of equations, and average over an observation window of length T to obtain expectations. Hence, the model coefficients are computed by solving the following linear equation:

$$R * A = B \tag{3}$$

where

$$R = \begin{pmatrix} \langle\, x^2 \,\rangle & \langle\, x_{\tau_1} x_{\tau_2} \,\rangle & \langle\, x_{\tau_1}^2 x_{\tau_2} \,\rangle \\ \langle\, x_{\tau_1} x_{\tau_2} \,\rangle & \langle\, x^2 \,\rangle & \langle\, x_{\tau_1} x_{\tau_2}^2 \,\rangle \\ \langle\, x_{\tau_1}^2 x_{\tau_2} \,\rangle & \langle\, x_{\tau_1} x_{\tau_2}^2 \,\rangle & \langle\, x_{\tau_1}^2 x_{\tau_2}^2 \,\rangle \end{pmatrix} \tag{4}$$

$$A = \begin{pmatrix} a_1 \\ a_2 \\ a_3 \end{pmatrix} \qquad B = \begin{pmatrix} \langle\, \dot{x} x_{\tau_1} \,\rangle \\ \langle\, \dot{x} x_{\tau_2} \,\rangle \\ \langle\, \dot{x} x_{\tau_1} x_{\tau_2} \,\rangle \end{pmatrix}, \tag{5}$$

and $\langle \cdot \rangle$ stands for the expectation value.

The main practical advantage of using Eq. (3) is that we can avoid directly estimating the signal derivatives, which is the main difficulty for noisy signals. Indeed, the correlation involving the signal derivative can be calculated instead from the derivative of the correlation function, i.e.

$$\langle \dot{x} x_{\tau_1} \rangle = \frac{d}{d\tau_1} \langle x x_{\tau_1} \rangle, \tag{6}$$

and

$$\langle \dot{x} x_{\tau_1} x_{\tau_2} \rangle = \frac{d}{d\tau_1} \langle x x_{\tau_1} x_{\tau_2} \rangle + \frac{d}{d\tau_2} \langle x x_{\tau_1} x_{\tau_2} \rangle. \tag{7}$$

These formulas are valid in the long window limit for a bounded stationary signal $x(t)$. We note that the expectation values on the left hand side of Eq. (3) can be written as the standard higher-order data moment functions [4]. For example, $\langle x_{\tau_1} x_{\tau_2}^2 \rangle = m_{xxx}(\tau_2 - \tau_1, \tau_2 - \tau_1)$ where the 3rd order moment function is defined as $m_{xxx}(\tau_1, \tau_2) = \langle x(t) x(t - \tau_1) x(t - \tau_2) \rangle$ and describes bi-correlations. However, the dynamical moments involving $\dot{x}$ express information not utilized in standard higher order methods, and arise exactly because of the dynamical signal hypothesis.

3 Hypothesis Testing

In this Section we describe the Mahalanobis distance-based discrimination method which we will use later in our data analysis. For the simple detection problem, we assume that there are only two data classes: noise and signal. For each of these we make N_n and N_s observations, respectively, using a fixed window length. By applying the DDE model we obtain for each class a set of model coefficients $\left\{ \mathbf{A}_i^{(n)} \right\}_{i=1}^{N_n}$ and $\left\{ \mathbf{A}_i^{(s)} \right\}_{i=1}^{N_s}$ where the vector notation $\mathbf{A} = (a_1, a_2, a_3)'$ has been introduced. The detection problem now reduces to how well one can discriminate between these multi-variate feature distributions.

A systematic treatment of this discrimination problem was done in [5], who considered the definition of distance between multi-variate normal populations. While the distribution of the DDE model coefficients is typically not Gaussian, for low-SNR they are nearly so. We have found that alternative methods that do not rely on the normality assumption, e.g. logistic discrimination [6], do not show significant improvement over the Mahalanobis method when the signal-to-noise ratio is very low.

Thus, for each independent realization $\mathbf{A}$ we compute the squared Mahalanobis distance

$$\Delta(\mathbf{A}) = \left(\bar{\mathbf{A}}^{(s)} - \bar{\mathbf{A}}^{(n)} \right)' \; \mathbf{\Sigma}^{-1} \; \left(\mathbf{A} - \bar{\mathbf{A}} \right). \tag{8}$$

Here $\mathbf{\Sigma}$ is the common covariance matrix approximated by $\mathbf{\Sigma} = (\mathbf{\Sigma}_s + \mathbf{\Sigma}_n)/(N_s + N_n)$, $\bar{\mathbf{A}}^{(s)}$ and $\bar{\mathbf{A}}^{(n)}$ are the mean of the distributions for the signal and noise classes respectively, and $\bar{\mathbf{A}} = \left(\bar{\mathbf{A}}^{(s)} - \bar{\mathbf{A}}^{(n)}\right)/2$. In practical cases the means and the covariance matrix are unknown and have to be estimated from a training set, unless the analytic signal forms are known.

To perform hypothesis testing on new observations, we use the Matusita allocation principle [7], defined by the following discrimination rule for the unknown observation $\mathbf{A}$:

$$\text{if } \Delta(\mathbf{A}) \begin{cases} \geq 0, & \text{allocate } \mathbf{A} \text{ to the signal class} \\ < 0, & \text{allocate } \mathbf{A} \text{ to the noise class} \end{cases} \tag{9}$$

The Matusita allocation principle as formulated in (9) leads to an optimal separation between the two distributions, but results in a fixed false alarm rate. The false alarm rate, however, is often specified by operational design, and therefore the detector has to be modified to include a threshold distance:

$$\text{if } \Delta(\mathbf{A}) \begin{cases} \geq \Delta_c, & \text{allocate } \mathbf{A} \text{ to the signal class} \\ < \Delta_c, & \text{allocate } \mathbf{A} \text{ to the noise class} \end{cases} \tag{10}$$

where the threshold distance Δ_c is set to obtain the preset false alarm rate P_{fa}. If $\mathcal{P}^{(n)}(\Delta)$ is the estimated probability density function for the noise sample then the condition for Δ_c is

$$\int_{\Delta_c}^{\infty} \mathcal{P}^{(n)}(\Delta)\, d\Delta = P_{fa}. \tag{11}$$

Using the discrimination principle (10) we are able to generate performance estimates for various detection scenarios.

4 Hybrid Detector

Since the dynamical detector is insensitive to signal power, we also design a hybrid detector. The hybrid detector is a combination of the dynamical detector and the band-matched energy detector. We simply use a four dimensional feature space constituted by the three model parameters (i.e. a_1, a_2, and a_3) and the signal energy. The output decision can then be made with Mahalanobis distance as described in the previous section.

We made a numerical experiment, in which both the noise and the signal were generated by a white Gaussian process, only their energy content were different. Since the signal is truly random the dynamical detector should not provide any detection and hence the hybrid detector performance should be identical to the energy detector. In Fig. 1 the ROC curve for the energy, dynamical and hybrid detector are displayed and we observe the expected behavior.

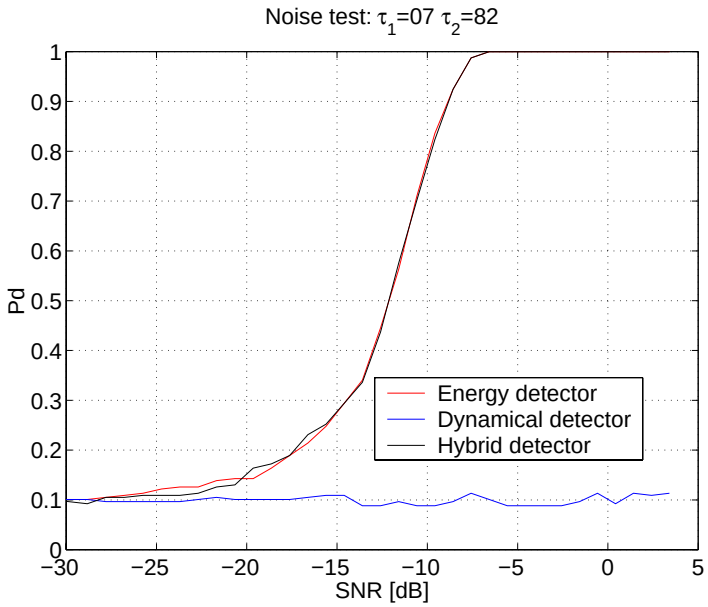

Figure 1: *Numerically estimated detection probabilities Pd vs. signal-to-noise ratio (SNR) for the noise test using the dynamical detector, energy detector and hybrid detector. We use the delays* $\tau_1 = 7$ *and* $\tau_2 = 82$.

5 Sonar Data

Experimental sea trials were performed by the Swedish Defense Research Agency in the Baltic Sea, which contributed to the acoustic data set analyzed here. The experiments were performed in waters of approximately constant depth of 30 m using a 23 ft fiberglass motor boat powered by a 4-cylinder, 4-stroke turbo charged Volvo-Penta (VP) diesel engine (type AD31P-A) having a VP Aquamatic stern drive (type AD31/DP) with an engine/drive gear ratio of 2.3:1. The stern drive was equipped with two counter rotating propellers (VP type A7) with 3 (front) and 4 (rear) blades. The sound propagated through the water was recorded with a passive hydrophone array, of which one hydrophone located at a depth of 17 m is used in the subsequent analysis presented in this report. All data was sampled at a rate of 25 kHz (no prefiltering), which was considered sufficient since virtually all the power in the signals and noise was confined to the frequency region below 5 kHz. In Fig. 2 a sketch of the test site is displayed.

In each recording the boat was run on constant throttle on a straight-track path passing directly above the hydrophone (see Fig. 2). The data analyzed here were taken from a time frame with the closest point of approach (CPA) corresponding to the middle of the frame. Moreover, ambient noise was recorded using the hydrophone array both before and after the sea trial.

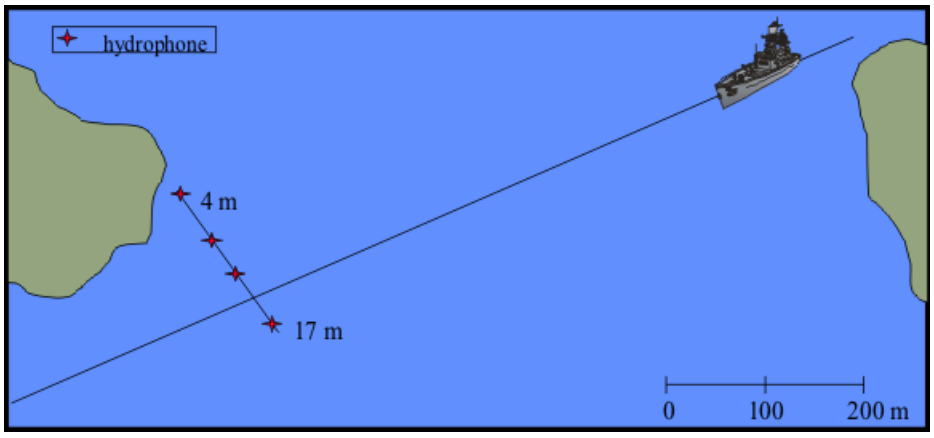

Figure 2: *The test site*

In Fig. 3 to Fig. 6 representative time-series and power spectra from the 1500, 2000 ,3000 and the 4000 RPM recordings are displayed.

This data was in part previously analyzed by the Swedish Defence Research Agency using higher-order spectral techniques. This analysis showed that by using the skewness (a normalized version of the bispectrum) it is possible to find coupled frequencies that could be generated by quadric phase coupling. In Fig. 7 the skewness is displayed for the 3000 RPM recording. For more details on this

analysis the reader is referred to [8].

These results seem to indicate interesting mechanical processes contributing to the acoustic signatures. Here we attempt to exploit these using our dynamical detectors.

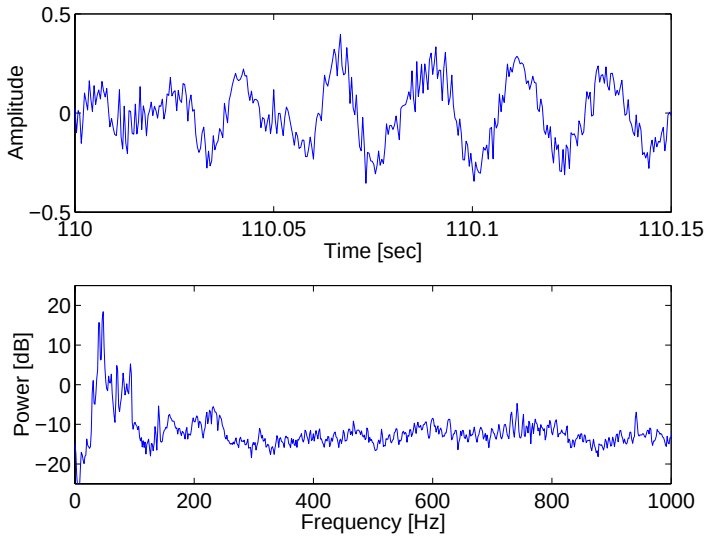

Figure 3: *Time-series (top) and power spectrum (bottom) from the 1500 RPM recording.*

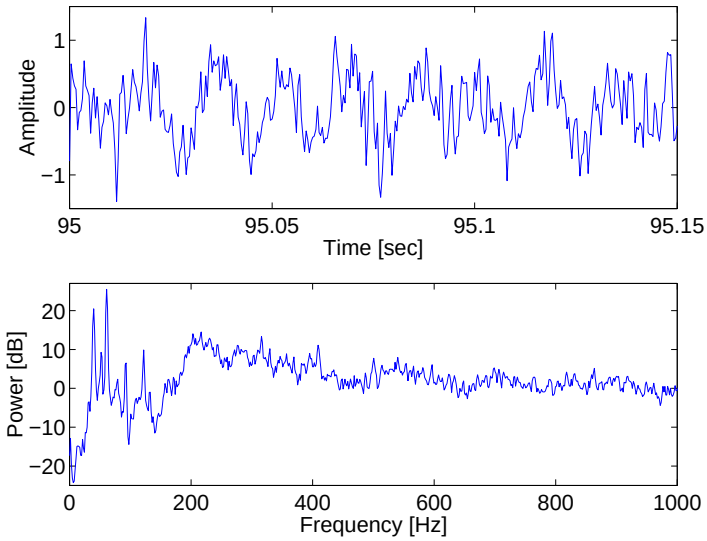

Figure 4: *Time-series (top) and power spectrum (bottom) from the 2000 RPM recording.*

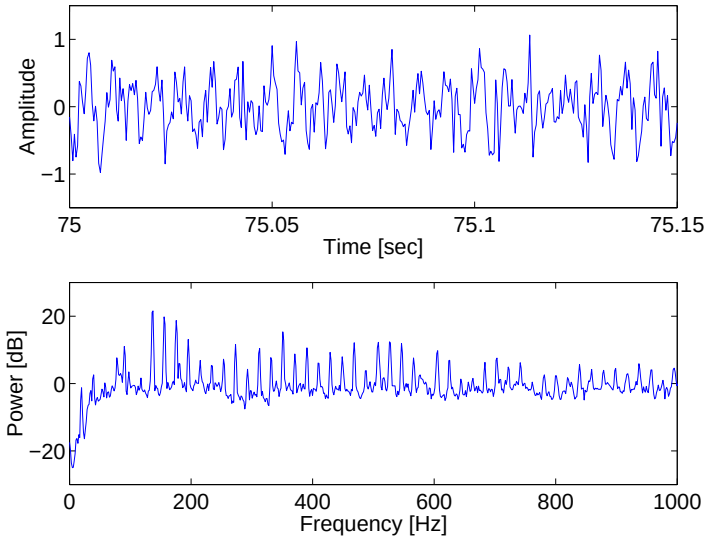

Figure 5: *Time-series (top) and power spectrum (bottom) from the 3000 RPM recording.*

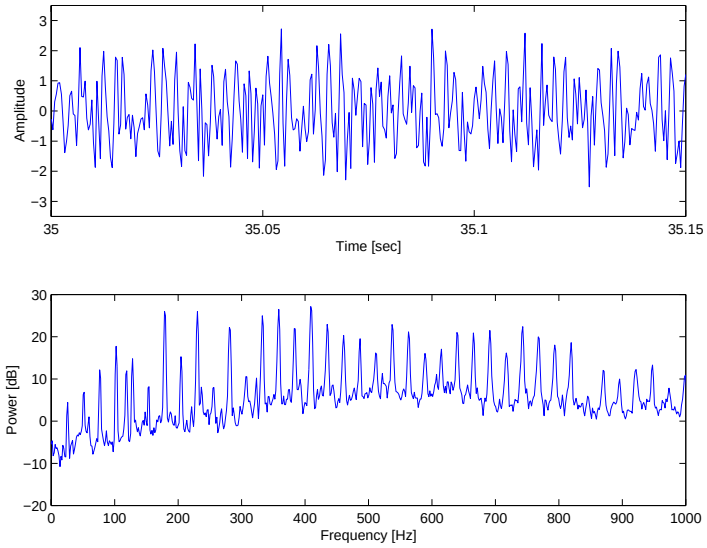

Figure 6: *Time-series (top) and power spectrum (bottom) from the 4000 RPM recording.*

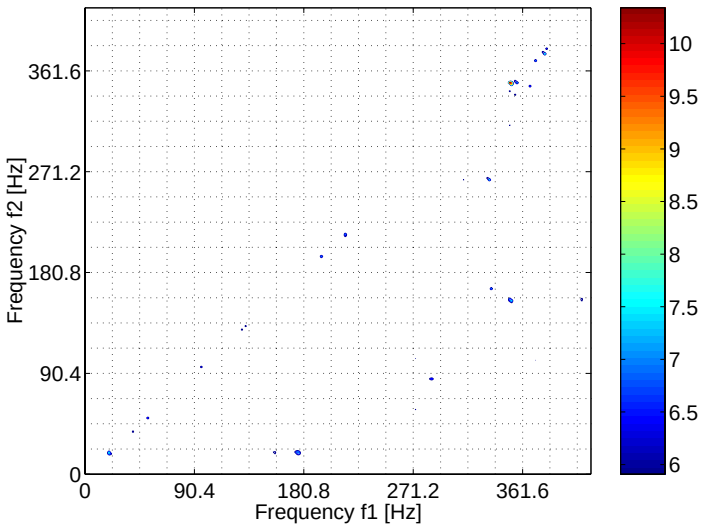

Figure 7: *Skewness for the 3000 RPM recording.*

6 Detection Test

Here we numerically implement the dynamical detector on the sonar data and compare the results with a band-matched energy detector. For the analysis here we build both RPM specific detectors and RPM independent detectors, for four different RPMs, namely 1500, 2000, 3000 and 4000. Note that these different RPM ranges correspond to different boat dynamics, such as engine loading and hydrofoiling, which somewhat change the acoustic properties in the far field, hence it is of interest to examine detection performance for all RPM ranges. We analyze a 15 seconds segment around the closest-point-of-approach (CPA) from each recording. As a background noise sample we use a one minute sea noise segment recorded in quiet water after the boat experiments. To preprocess the data we low-pass filtered the signal using a Chebyshev filter with the cut-off frequency at 1250 Hz. To obtain our features we estimated the dynamical model with a window length of 0.5 seconds for a sampling rate of 25 kHz (12,500 samples) and the window was shifted by 0.25 seconds (6250 samples). By using the DDE model of Eq. (2) and the estimation procedure of Section 2, we computed the model coefficients for the selected data segments. Using the feature distributions generated from the data as above, we next implemented the Mahalanobis decision criteria described in Section 3 to design a detector, choosing a fixed false alarm rate of $P_{fa} = 0.1$ as a design parameter.

As a benchmark, we compared to a frequency band-matched energy detector which monitors the signal power below 1 kHz, where most of the boat signatures are located. We note here that knowing the boat type and the exact RPM one could design a more sensitive energy detector which monitors only certain frequency bins. However, such detailed information is usually not available in an operational environment and therefore the comparison with the energy detector tuned to the full 0-1 kHz band provides a more realistic benchmark. In addition, we also estimate the detection performance of the hybrid detector and compare it to the other two detectors. All detectors are designed with a fixed false alarm rate $P_{fa} = 0.1$.

To calculate the detection performance as a function of varying SNR levels we artificially degraded the signal by adding additional re-scaled sea noise recorded after the experiments. First, the hydrophone recordings are scaled such that the ocean noise n is a zero mean, unit variance signal. Since the recording of the boat noise x also contains the same level of sea noise, the artificially degraded signal is defined as

$$y = \frac{x + c\, n}{\sqrt{1 + c^2}}, \tag{12}$$

where $c = 10^{-SNR_F/20}$ and SNR_F is the "full bandwidth" SNR. One can observe that for a large SNR_F ($c \to 0$) the variance of the degraded signal y is close to the variance of x, while in the limit of small SNR_F ($c \to \infty$) the variance of y

is the same as the variance of the noise. This ensures proper calibration of the energy of the degraded signal, which is important for the accurate calculation of the energy detector's performance.

Since nearly all of the boat signatures are located below 1 kHz, for a more accurate determination of the SNR we will use the following formula

$$SNR\ (dB) = 10\ \log_{10}\left(\frac{\mathcal{P}_f(y)}{\mathcal{P}_f(n)} - 1\right). \tag{13}$$

Where $\mathcal{P}_f(y)$ and $\mathcal{P}_f(n)$ stands for the signal and noise power below 1 kHz, respectively. The factor -1 arises due to the fact that y is not a clean signal but also contains the sea noise by default.

6.1 RPM Specific Detectors

In this section and the next we design two slightly different types of dynamical detectors in order to characterize their performance. For the first type, we design detectors which are optimized for each RPM value. For the second type, we design a single dynamical detector for all RPM values. We will see that the two types of detectors are generally close in terms of model parameters.

The delay differential equation models are characterized significantly by the delay time parameters, hence it is necessary to estimate good values for these parameters (in this case two delays) first. Generally, this involve some search procedure over a wide range of values, and comparison to some performance metric. Here we use two different methods to select the delays. For both methods we search all possible combinations of delays between 3 and 100 samples, which provides a large range of possible time scales.

Method 1:
This procedure simply calculates the deviation of the mean estimated model coefficients from the origin of the feature space, which is a rough measure of the statistical significance of the detection output. To do so, we use a subset (12.5 %) of each recording to select the delays from the maximum significance of L, where L is given by,

$$L = \sqrt{a_1^2(\tau_1, \tau_2) + a_2^2(\tau_1, \tau_2) + a_3^2(\tau_1, \tau_2)}. \tag{14}$$

and constitutes simply the vector distance of the mean coefficient distributions from the feature space origin. The time delays are then chosen which maximize this distance.

Method 2:
Here we calculate the time delays using a method which relies on maximizing the

output detection performance, and is thus a more direct and desirable metric. First, we determine the SNR of a signal for which the energy detector has some reasonable performance level, in this case a probability of detection of about 0.7. Using this SNR level, we then calculate the time delays which maximize the detection probability Pd for the dynamical detector. This method generally yields time delays somewhat different than the first method, and produce slightly better overall classification performance.

6.1.1 1500 RPM recording

Figure 8 shows the significance of L estimated from a subset of the 1500 RPM recording. The maximum significance of L is achieved with the delays $\tau_1 = 9$ and $\tau_2 = 18$ samples.

In Fig. 9 the ROC curves for the dynamical detector (delays selected with method 1) and the band-matched energy detector are displayed. As can be seen the dynamical detector shows a performance gain of 2-3 dB over the energy detector.

Figure 10 shows the numerically estimated detection probability Pd for the dynamical detector (1500 RPM recording) at a SNR at which the energy detector has $Pd = 0.68$. As can be seen the dynamical detector out performs the energy detector for a wide range of delay pairs. The maximum detection Pd for the dynamical detector is achieved for the delays $\tau_1 = 9$ and $\tau_2 = 91$ samples.

In Fig. 11 the ROC curves for the dynamical detector, the band-matched energy detector and the hybrid detector are displayed. The deleys for the dynamical and hybrid detector were selected with method 2. As can be seen the dynamical and hybrid detector shows a performance gain of 3-4 dB over the energy detector. In this case, since the dynamical detector performance is significantly greater than the energy detector, the later contributes very little to the hybrid detector performance.

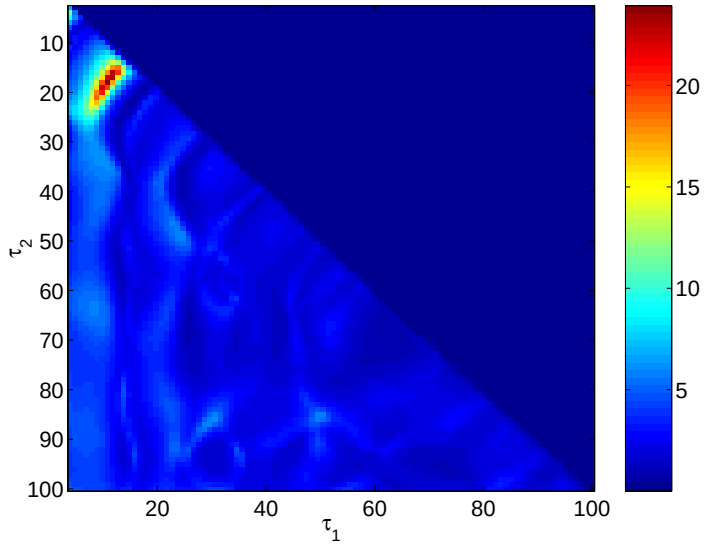

Figure 8: *Significance of L estimated from a subset of the 1500 RPM recording.*

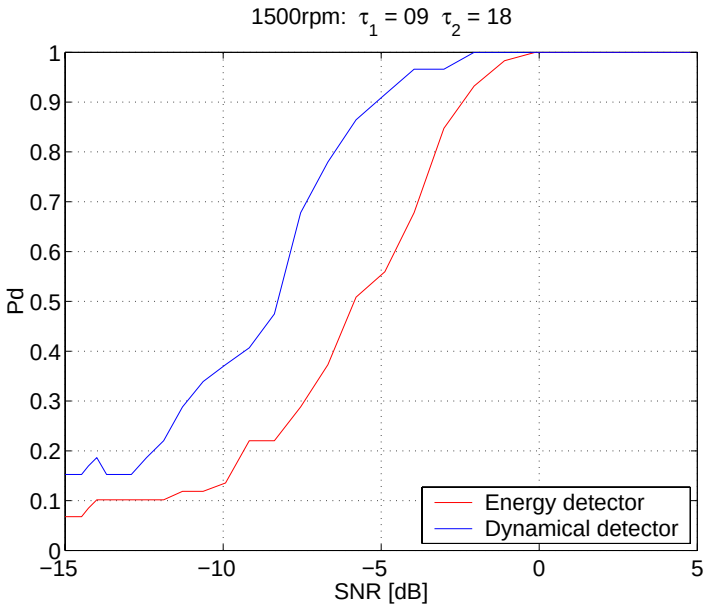

Figure 9: *Numerically estimated detection probabilities Pd vs. signal-to-noise ratio (SNR) for the 1500 RPM recording using the dynamical detector and energy detector. We use the delays $\tau_1 = 9$ and $\tau_2 = 18$, selected from the maximum significance of L.*

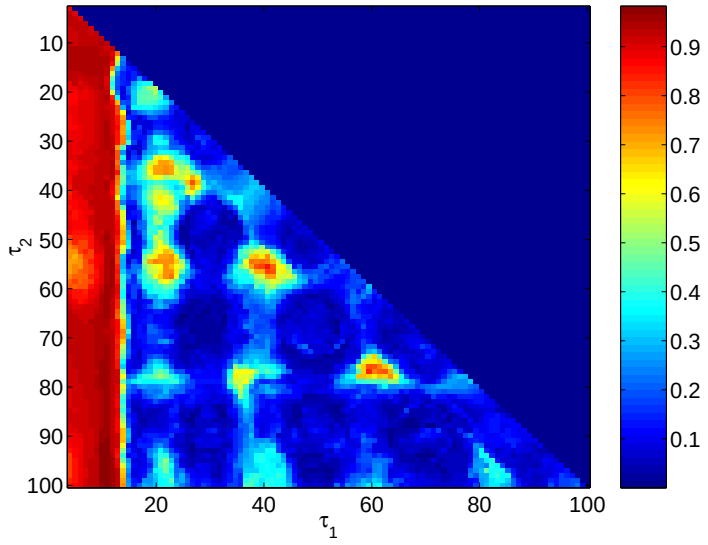

Figure 10: *Numerically estimated detection probabilities Pd for the dynamical detector for the 1500 RPM recording at a SNR at which the energy detector has* $Pd = 0.68$.

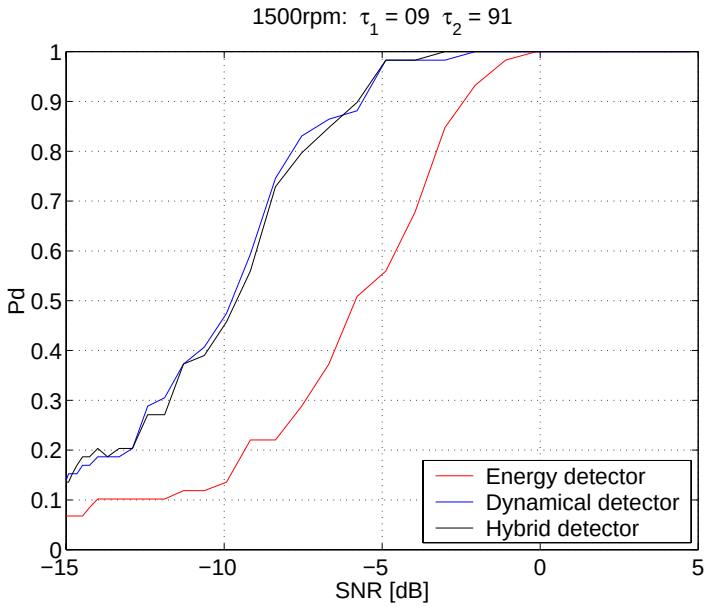

Figure 11: *Numerically estimated detection probabilities Pd vs. signal-to-noise ratio (SNR) for the 1500 RPM recording using the dynamical detector, energy detector and hybrid detector. We use the delays* $\tau_1 = 9$ *and* $\tau_2 = 91$ *selected from the maximum Pd for the dynamical detector when the energy detector has* $Pd = 0.68$.

6.1.2 2000 RPM recording

Figure 12 shows the significance of L estimated from a subset of the 2000 RPM recording. The maximum significance of L is achieved with the delays $\tau_1 = 11$ and $\tau_2 = 38$ samples.

In Fig. 13 the ROC curves for the dynamical detector (delays selected with method 1) and the band-matched energy detector are displayed. As can be seen the dynamical detector shows a performance gain of 2-3 dB over the energy detector.

Figure 14 shows the numerically estimated detection probability Pd for the dynamical detector (2000 RPM recording) at a SNR at which the energy detector has $Pd = 0.69$. As can be seen the dynamical detector out performs the energy detector for a wide range of delay pairs. The maximum detection Pd for the dynamical detector is achieved for the delays $\tau_1 = 5$ and $\tau_2 = 58$ samples.

In Fig. 15 the ROC curves for the dynamical detector, the band-matched energy detector and the hybrid detector are displayed. The deleys for the dynamical and hybrid detector were selected with method 2. As can be seen the dynamical and hybrid detector shows a performance gain of 2-3 dB over the energy detector. In this case, since the dynamical detector performance is significantly greater than the energy detector, the later contributes very little to the hybrid detector performance.

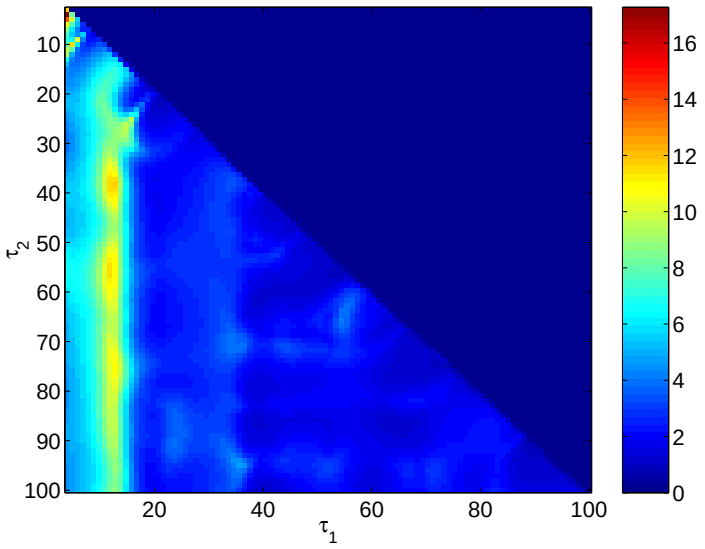

Figure 12: *Significance of L estimated from a subset of the 2000 RPM recording.*

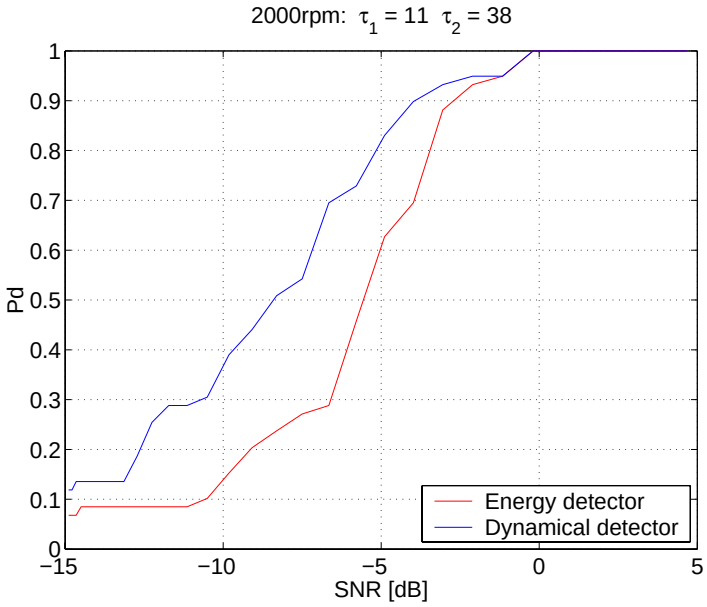

Figure 13: *Numerically estimated detection probabilities Pd vs. signal-to-noise ratio (SNR) for the 2000 RPM recording using the dynamical detector and energy detector. We use the delays* $\tau_1 = 11$ *and* $\tau_2 = 38$ *selected from the maximum significance of* L.

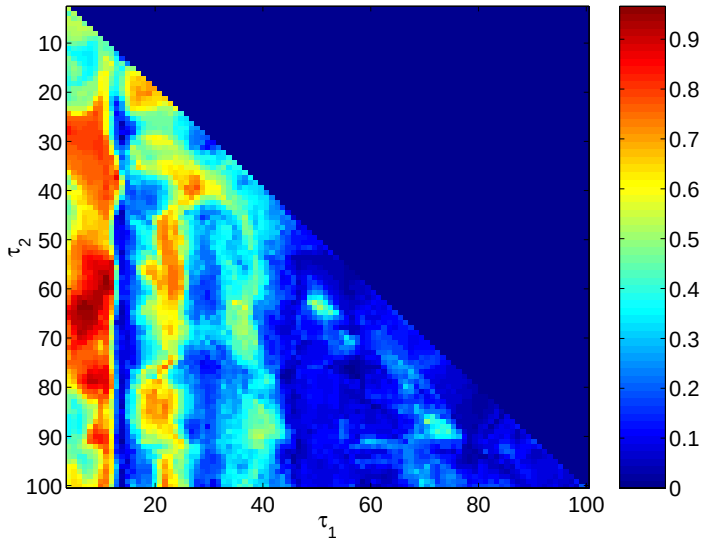

Figure 14: *Numerically estimated detection probabilities Pd for the dynamical detector for the 2000 RPM recording at a SNR at which the energy detector has* $Pd = 0.69$.

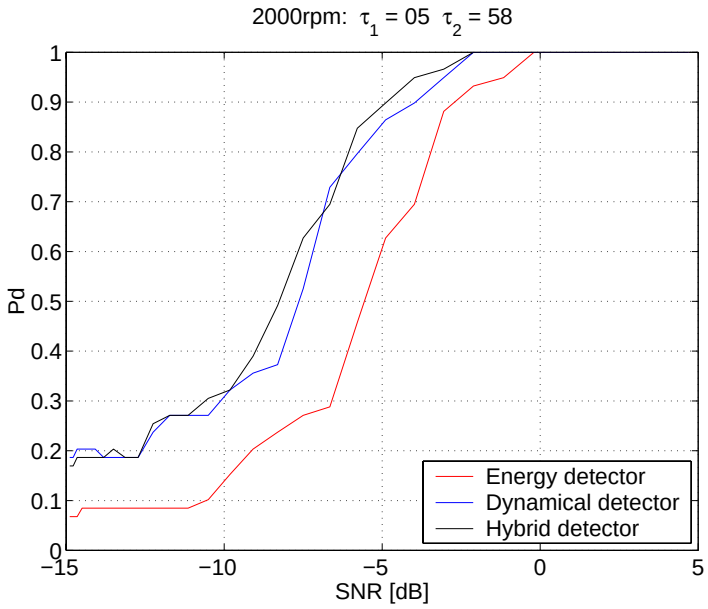

Figure 15: *Numerically estimated detection probabilities Pd vs. signal-to-noise ratio (SNR) for the 2000 RPM recording using the dynamical detector, energy detector and hybrid detector. We use the delays $\tau_1 = 5$ and $\tau_2 = 58$ selected from the maximum Pd for the dynamical detector when the energy detector has $Pd = 0.69$.*

6.1.3 3000 RPM recording

Figure 16 shows the significance of L estimated from a subset of the 3000 RPM recording. The maximum significance of L is achieved with the delays $\tau_1 = 9$ and $\tau_2 = 88$ samples.

In Fig. 17 the ROC curves for the dynamical detector (delays selected with method 1) and the band-matched energy detector are displayed. As can be seen the dynamical detector shows a performance gain of 3-5 dB over the energy detector.

Figure 18 shows the numerically estimated detection probability Pd for the dynamical detector (3000 RPM recording) at a SNR at which the energy detector has $Pd = 0.63$. As can be seen the dynamical detector out performs the energy detector for a wide range of delay pairs. The maximum detection Pd for the dynamical detector is achieved for the delays $\tau_1 = 7$ and $\tau_2 = 82$ samples.

In Fig. 19 the ROC curves for the dynamical detector, the band-matched energy detector and the hybrid detector are displayed. The deleys for the dynamical and hybrid detector were selected with method 2. As can be seen the dynamical and hybrid detector shows a performance gain of 4-5 dB over the energy detector. In this case, since the dynamical detector performance is significantly greater than the energy detector, the later contributes very little to the hybrid detector performance.

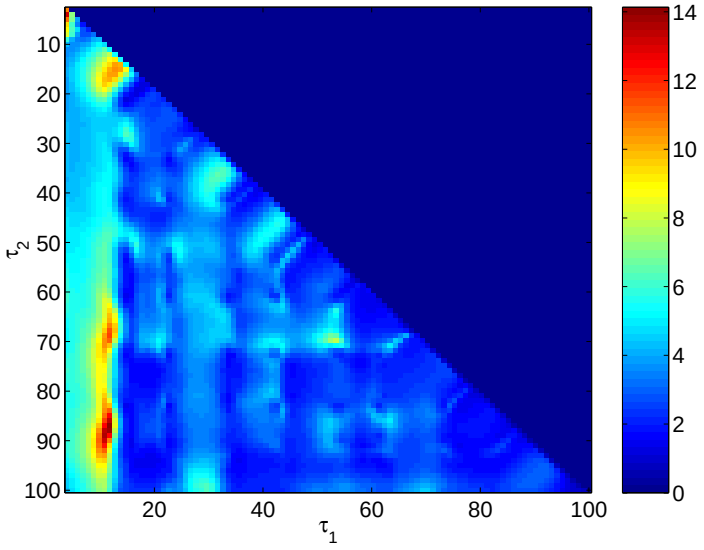

Figure 16: *Significance of L estimated from a subset of the 3000 RPM recording.*

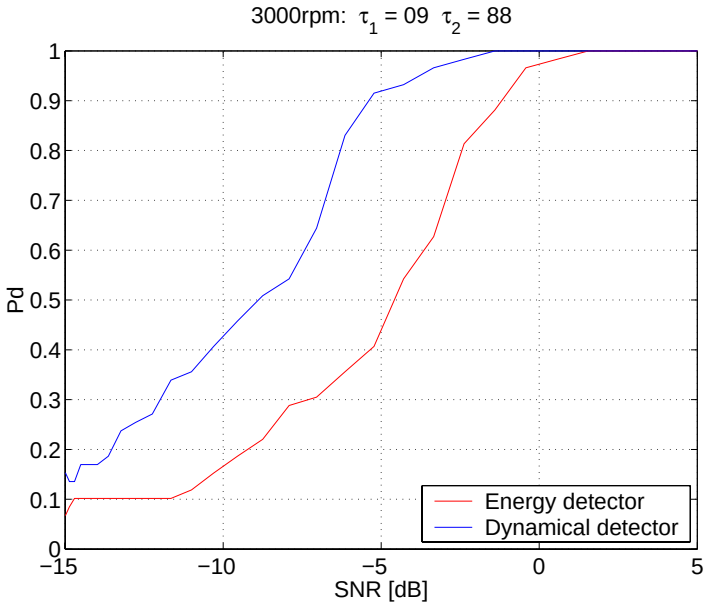

Figure 17: *Numerically estimated detection probabilities Pd vs. signal-to-noise ratio (SNR) for the 3000 RPM recording using the dynamical detector and energy detector. We use the delays* $\tau_1 = 9$ *and* $\tau_2 = 88$ *selected from the maximum significance of* L.

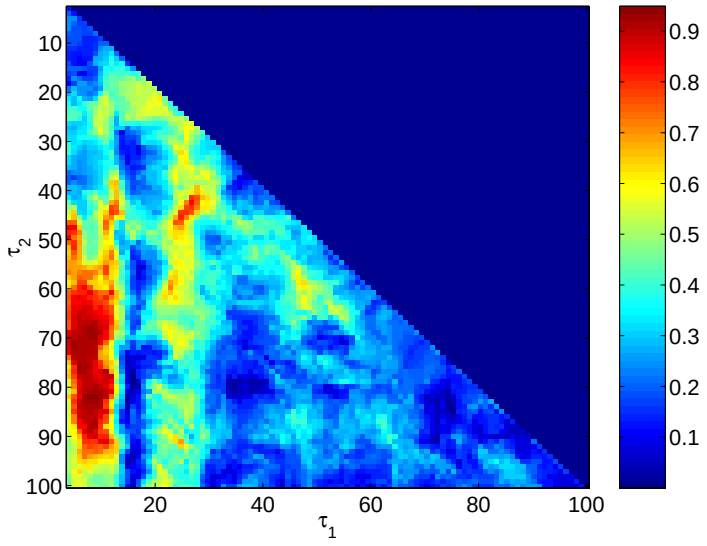

Figure 18: *Numerically estimated detection probabilities Pd for the dynamical detector for the 3000 RPM recording at a SNR at which the energy detector has* $Pd = 0.63$.

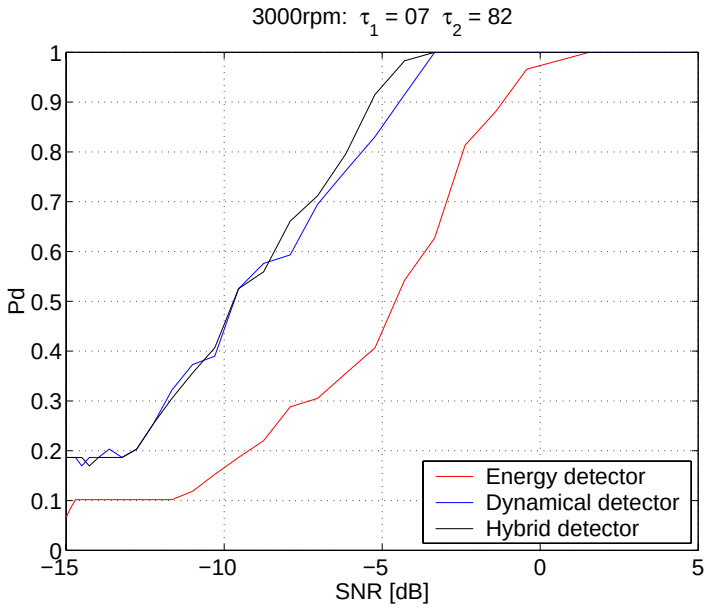

Figure 19: *Numerically estimated detection probabilities Pd vs. signal-to-noise ratio (SNR) for the 3000 RPM recording using the dynamical detector, energy detector and hybrid detector. We use the delays $\tau_1 = 7$ and $\tau_2 = 82$ selected from the maximum Pd for the dynamical detector when the energy detector has $Pd = 0.63$.*

6.1.4 4000 RPM recording

Figure 20 shows the significance of L estimated from a subset of the 4000 RPM recording. The maximum significance of L is achieved with the delays $\tau_1 = 7$ and $\tau_2 = 32$ samples.

In Fig. 21 the ROC curves for the dynamical detector (delays selected with method 1) and the band-matched energy detector are displayed. In this case the dynamical detector does not show a performance gain over the energy detector.

Figure 22 shows the numerically estimated detection probability Pd for the dynamical detector (4000 RPM recording) at a SNR at which the energy detector has $Pd = 0.69$. The maximum detection Pd for the dynamical detector is achieved for the delays $\tau_1 = 13$ and $\tau_2 = 21$ samples.

In Fig. 23 the ROC curves for the dynamical detector, the band-matched energy detector and the hybrid detector are displayed. The deleys for the dynamical and hybrid detector were selected with method 2. As can be seen the dynamical detector shows a performance gain of 1-2 dB over the energy detector. In this case since the dynamical detector performance is not significantly better than the energy detector, the hybrid detector shows additional gain over the energy detector.

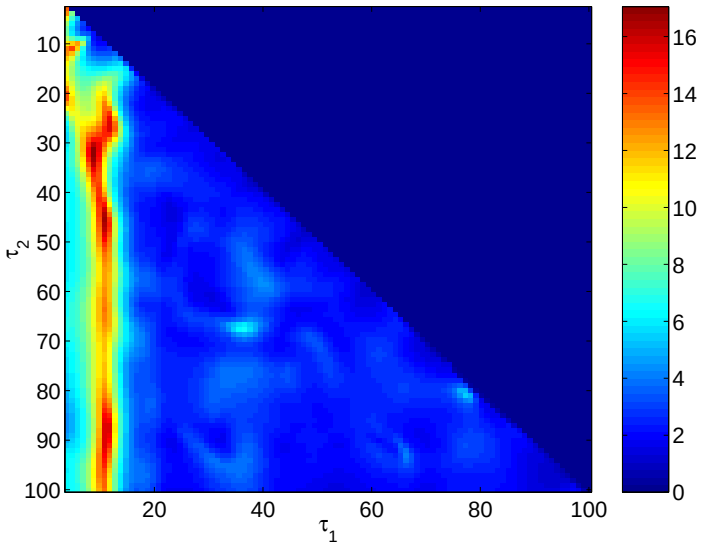

Figure 20: *Significance of L estimated from a subset of the 4000 RPM recording.*

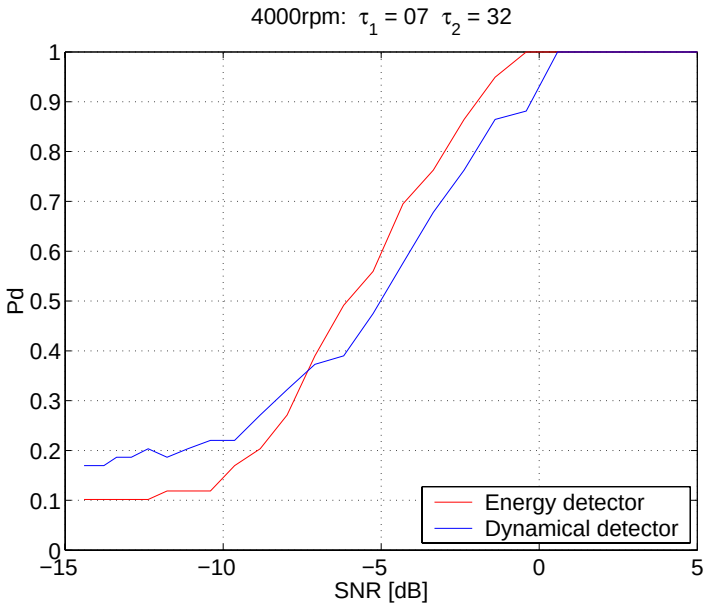

Figure 21: *Numerically estimated detection probabilities Pd vs. signal-to-noise ratio (SNR) for the 4000 RPM recording using the dynamical detector and energy detector. We use the delays* $\tau_1 = 7$ *and* $\tau_2 = 32$ *selected from the maximum significance of L.*

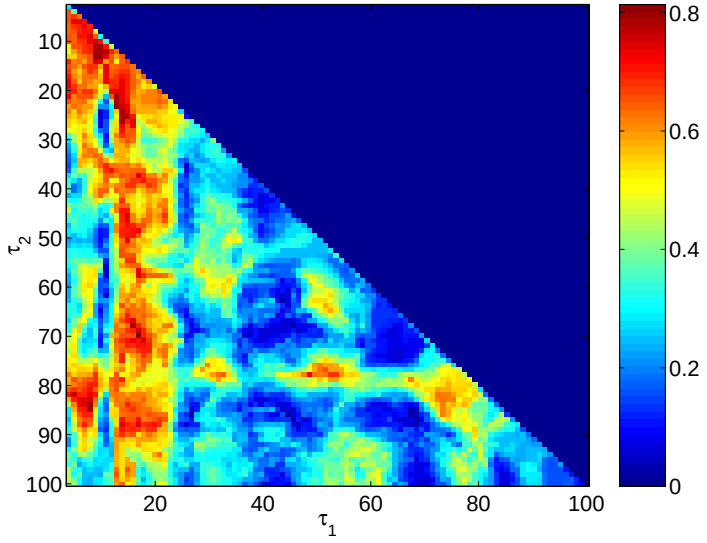

Figure 22: *Numerically estimated detection probabilities Pd for the dynamical detector for the 4000 RPM recording at a SNR at which the energy detector has* $Pd = 0.69$.

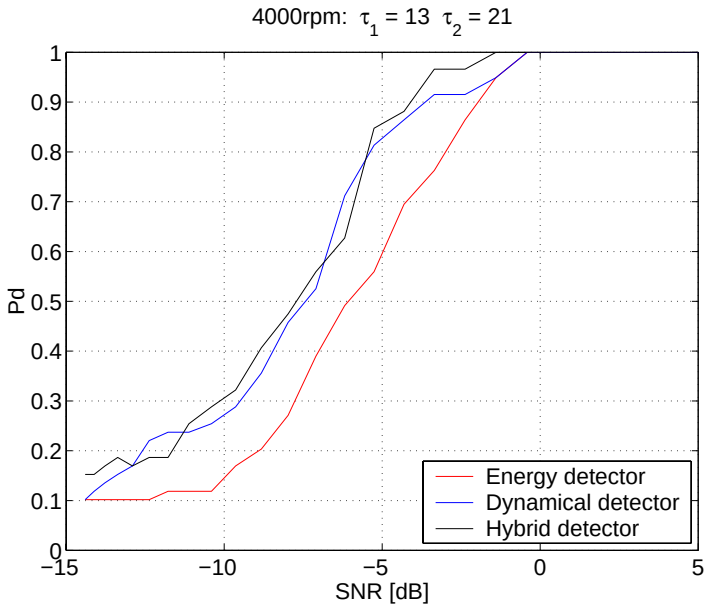

Figure 23: *Numerically estimated detection probabilities Pd vs. signal-to-noise ratio (SNR) for the 4000 RPM recording using the dynamical detector, energy detector and hybrid detector. We use the delays $\tau_1 = 13$ and $\tau_2 = 21$ selected from the maximum Pd for the dynamical detector when the energy detector has $Pd = 0.69$.*

6.2 RPM Independent Detectors

In this section we aim to design RPM independent dynamical detectors, i.e. we select one model time delay pair which provides the maximum average detection performance over all input RPM values. The idea is to try to design a robust detector which gives reasonable performance for any data set.

In order to select the RPM independent delays, we first calculate the SNR levels at which the detection probability for the energy detector is approximately 0.7 for each RPM, as in the previous section. We next calculate the corresponding detection probabilities of the dynamical detector for all four RPM values, and average them. The model time delays are then chosen to maximize this average detection probability.

We also designed two different detectors, one for all four RPMs and one for all RPMs except 4000 RPM. The reason for excluding the 4000 RPM recording is that the dynamical detectors that were designed for the 4000 RPM recording in the previous section did not show reasonable performance due to amplitude clipping in some of the 4000 RPM data segments. Hence we calculated performance for both sets of data to gain more insight.

6.2.1 For the 1500, 2000, 3000 and 4000 RPM recordings

Figure 24 shows the average numerically estimated detection probabilities for the dynamical detectors for the 1500, 2000, 3000 and 4000 RPM recordings at SNRs at which the energy detectors have $Pd = 0.68$, $Pd = 0.69$, $Pd = 0.63$ and $Pd = 0.69$, respectively. The maximum average Pd for the dynamical detectors is achieved with $\tau_1 = 8$ and $\tau_2 = 79$.

In Fig. 25 the ROC curves for the dynamical, energy and the hybrid detector for the 1500 RPM recording are displayed. The delays for the dynamical and hybrid detectors are chosen from the maximum average Pd for all 4 RPMs. As can be seen the dynamical detector and the hybrid detector shows a performance gain of 2-3 dB over the energy detector. In this case, since the dynamical detector performance is significantly greater than the energy detector, the later contributes very little to the hybrid detector performance.

In Fig. 26 the ROC curves for the dynamical, energy and the hybrid detector for the 2000 RPM recording are displayed. The delays are chosen from the maximum average Pd for all 4 RPMs. As can be seen the dynamical detector and the hybrid detector shows a performance gain of 2-3 dB over the energy detector. In this case, since the dynamical detector performance is significantly greater than the energy detector, the later contributes very little to the hybrid detector performance.

In Fig. 27 the ROC curves for the dynamical, energy and the hybrid detector for the 3000 RPM recording are displayed. The delays for the dynamical and hybrid detectors are chosen from the maximum average Pd for all 4 RPMs. As can be seen the dynamical detector and the hybrid detector shows a performance gain of 2-3 dB over the energy detector. In this case, since the dynamical detector performance is significantly greater than the energy detector, the later contributes very little to the hybrid detector performance.

In Fig. 28 the ROC curves for the dynamical, energy and the hybrid detector for the 4000 RPM recording are displayed. The delays for the dynamical and hybrid detector are chosen from the maximum average Pd for all 4 RPMs. In this case the dynamical detector and the energy detector have basically identical detection performance. The hybrid detector shows a performance gain of 1-2 dB over the other two detectors.

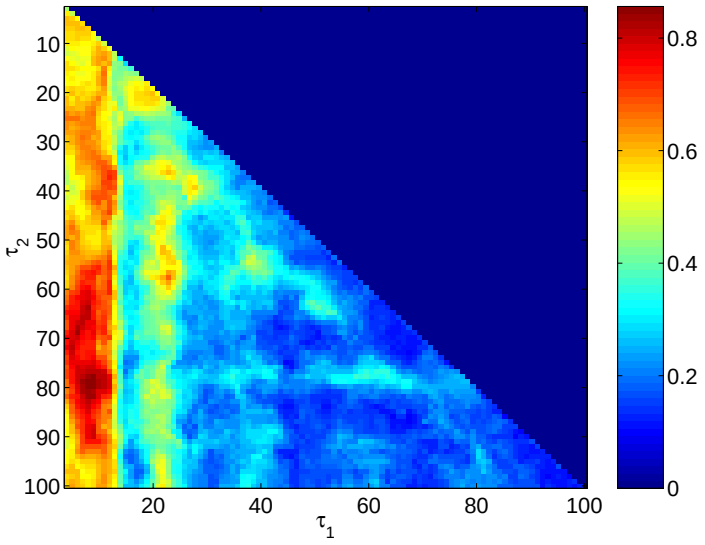

Figure 24: *Numerically estimated detection probabilities Pd for the dynamical detector for the 1500, 2000, 3000 and 4000 RPM recordings at SNRs at which the energy detectors have* $Pd = 0.68$, Pd*=0.69,* $Pd = 0.63$ *and* $Pd = 0.69$, *respectively.*

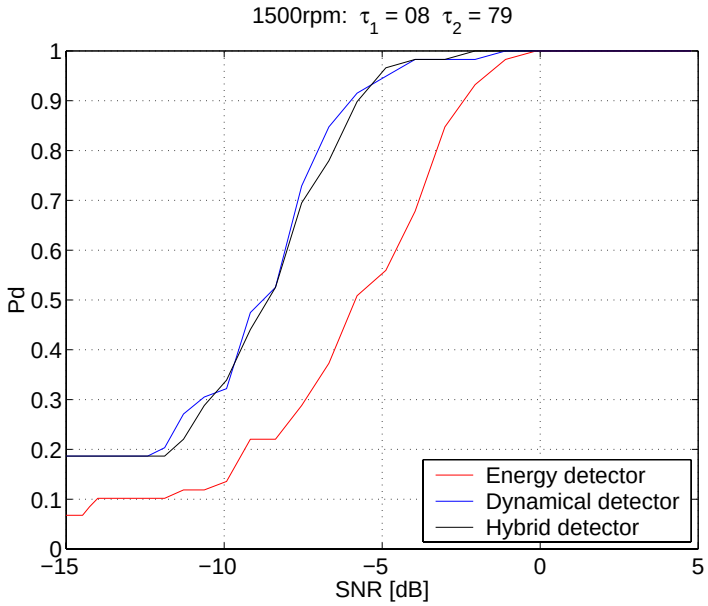

Figure 25: *Numerically estimated detection probabilities Pd vs. signal-to-noise ratio (SNR) for the 1500 RPM recording using the dynamical detector, energy detector and hybrid detector. We use the delays* $\tau_1 = 8$ *and* $\tau_2 = 79$.

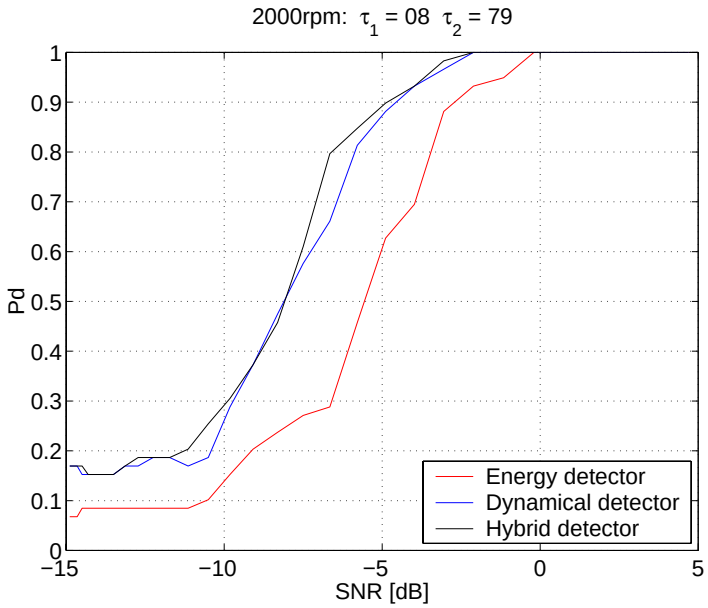

Figure 26: *Numerically estimated detection probabilities Pd vs. signal-to-noise ratio (SNR) for the 2000 RPM recording using the dynamical detector, energy detector and hybrid detector. We use the delays* $\tau_1 = 8$ *and* $\tau_2 = 79$.

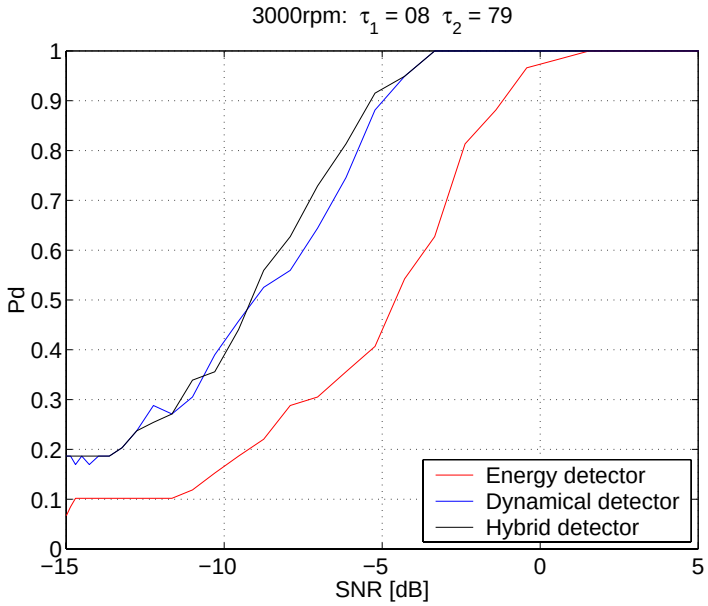

Figure 27: *Numerically estimated detection probabilities Pd vs. signal-to-noise ratio (SNR) for the 3000 RPM recording using the dynamical detector, energy detector and hybrid. We use the delays* $\tau_1 = 8$ *and* $\tau_2 = 79$.

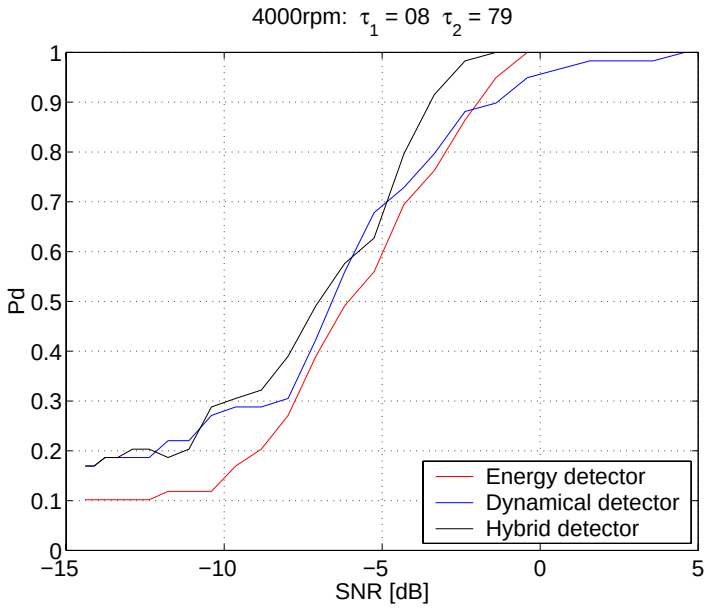

Figure 28: *Numerically estimated detection probabilities Pd vs. signal-to-noise ratio (SNR) for the 4000 RPM recording using the dynamical detector, energy detector and hybrid. We use the delays* $\tau_1 = 8$ *and* $\tau_2 = 79$.

6.2.2 For the 1500, 2000 and 3000 RPM recordings

Figure 29 shows the average numerically estimated detection probabilities for the dynamical detectors for the 1500, 2000 and 3000 RPM recordings at SNRs at which the energy detectors have $Pd = 0.68$, $Pd = 0.69$ and $Pd = 0.63$, respectively. The maximum average Pd for the dynamical detectors is achieved with $\tau_1 = 7$ and $\tau_2 = 67$.

In Fig. 30 the ROC curves for the energy, dynamical, and hybrid detector for the 1500 RPM recording are displayed. The delays are chosen from the maximum average Pd for the 1500, 2000 and 3000 RPM recordings. As can be seen the dynamical detector and the hybrid detector shows a performance gain of 2-4 dB over the energy detector. In this case, since the dynamical detector performance is significantly greater than the energy detector, the later contributes very little to the hybrid detector performance.

In Fig. 31 the ROC curves for the energy, dynamical, and hybrid detector for the 2000 RPM recording are displayed. The delays are chosen from the maximum average Pd for the 1500, 2000 and 3000 RPM recordings. As can be seen the dynamical detector and the hybrid detector shows a performance gain of 3-5 dB over the energy detector. In this case, since the dynamical detector performance is significantly greater than the energy detector, the later contributes very little to the hybrid detector performance.

In Fig. 32 the ROC curves for the energy, dynamical, and hybrid detector for the 3000 RPM recording are displayed. The delays are chosen from the maximum average Pd for the 1500, 2000 and 3000 RPM recordings. As can be seen the dynamical detector and the hybrid detector shows a performance gain of 4-6 dB over the energy detector. In this case, since the dynamical detector performance is significantly greater than the energy detector, the later contributes very little to the hybrid detector performance.

In Fig. 33 the ROC curves for the energy, dynamical, and hybrid detector for the 4000 RPM recording are displayed. The delays are chosen from the maximum average Pd for the 1500, 2000 and 3000 RPM recordings. As can be seen the dynamical detector does not provide any performance gain over the energy detector. The hybrid detector shows a performance gain of 1-2 dB over the other two detectors.

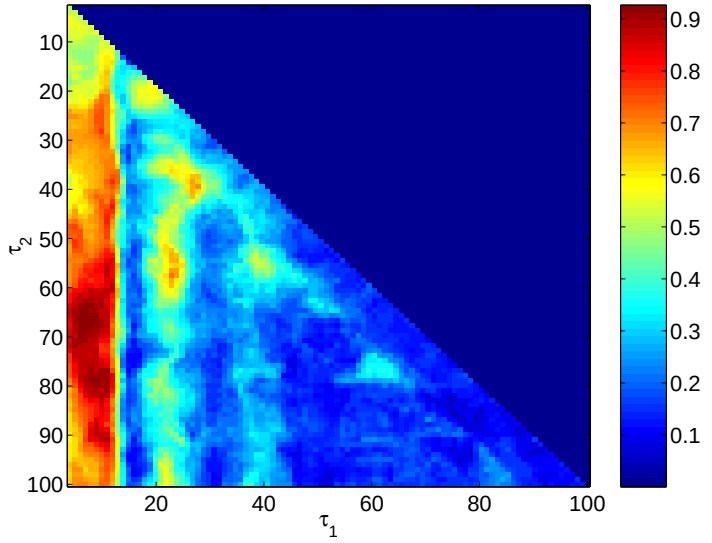

Figure 29: *Numerically estimated detection probabilities Pd for the dynamical detector for the 1500, 2000 and 3000 RPM recordings at SNRs at which the energy detectors have $Pd = 0.68$, $Pd = 0.69$ and $Pd = 0.63$, respectively.*

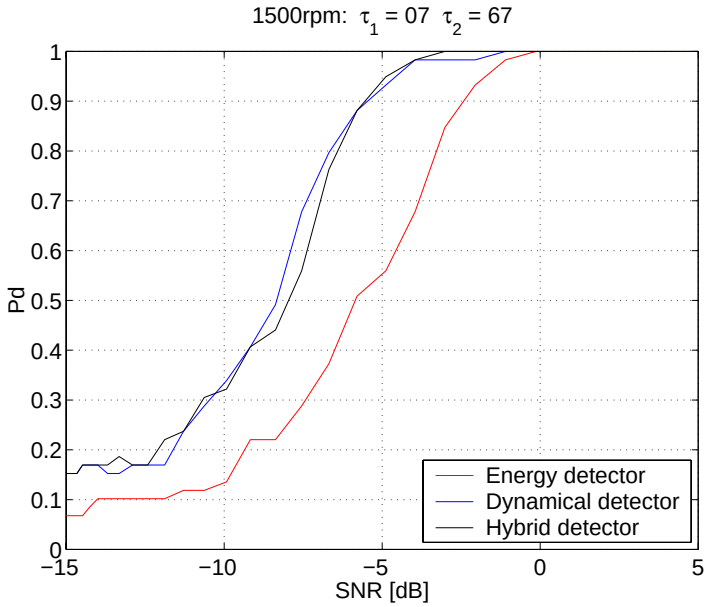

Figure 30: *Numerically estimated detection probabilities Pd vs. signal-to-noise ratio (SNR) for the 1500 RPM recording using the dynamical detector, energy detector and hybrid detector. We use the delays $\tau_1 = 7$ and $\tau_2 = 67$.*

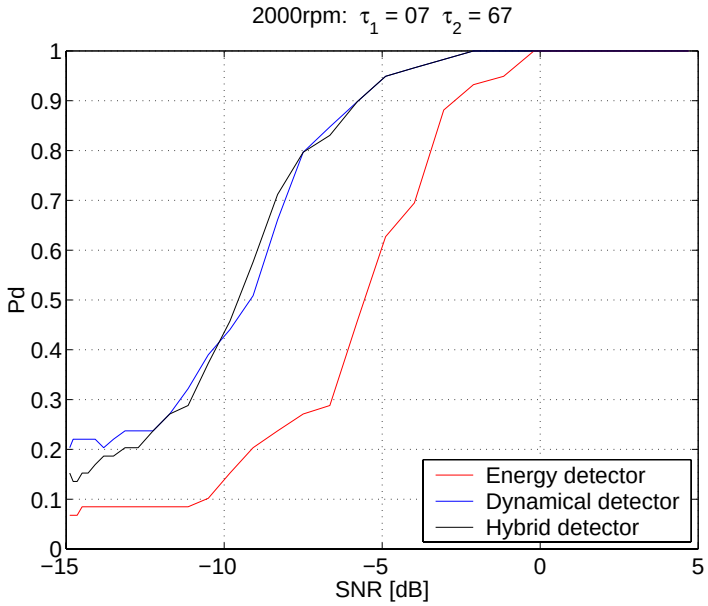

Figure 31: *Numerically estimated detection probabilities Pd vs. signal-to-noise ratio (SNR) for the 2000 RPM recording using the dynamical detector, energy detector and hybrid detector. We use the delays* $\tau_1 = 7$ *and* $\tau_2 = 67$.

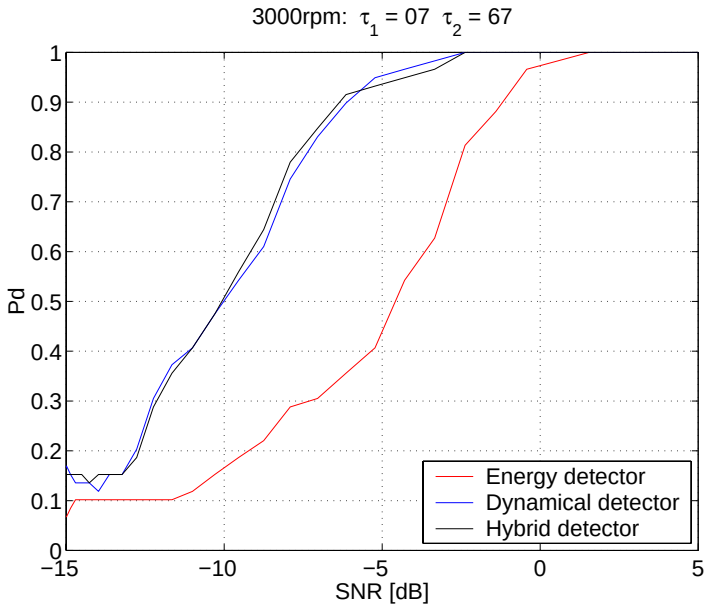

Figure 32: *Numerically estimated detection probabilities Pd vs. signal-to-noise ratio (SNR) for the 3000 RPM recording using the dynamical detector, energy detector and hybrid detector. We use the delays* $\tau_1 = 7$ *and* $\tau_2 = 67$.

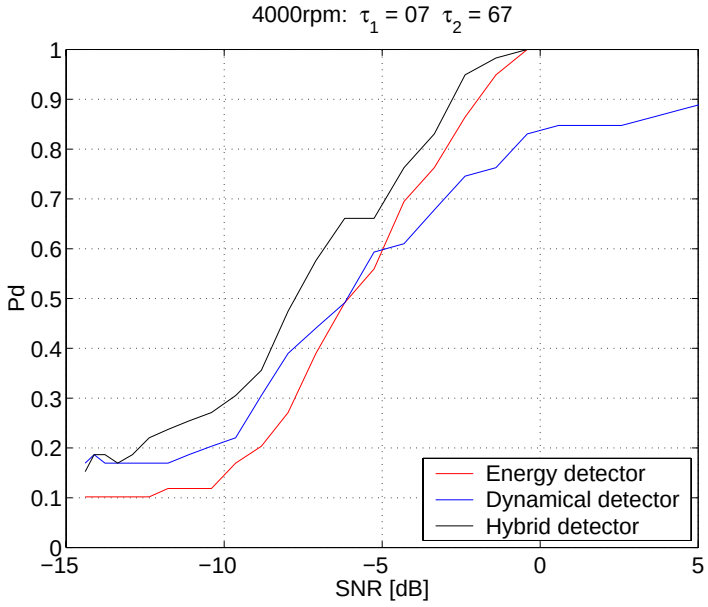

Figure 33: *Numerically estimated detection probabilities Pd vs. signal-to-noise ratio (SNR) for the 4000 RPM recording using the dynamical detector, energy detector and hybrid detector. We use the delays* $\tau_1 = 7$ *and* $\tau_2 = 67$.

7 Conclusions

In this report we presented an acoustic detection study of real-world sonar data, derived from a closely controlled sea trial in the Baltic Sea. In this study we designed detectors based on the dynamical model approach, combined with the Mahalanobis distance-based decision criteria. To benchmark the detection performance we compared the dynamical detector to a band matched energy detector. Since the dynamical detector is insensitive to signal amplitude, we also designed a hybrid detector which combined three dynamical model features with an energy feature, and estimated performance using this four-dimensional feature space. In a practical system, the hybrid detector would provide the best performance for all possible signal classes encountered.

We have designed both RPM specific and RPM independent dynamical detectors, depending on whether one wishes to maximize performance for a particular boat's RPM operational range or not, respectively. We generally found a performance gain for the dynamical detector of 2-6 dB over the band passed energy detector in almost all cases. It was only for the 4000 RPM recording that we could not show a significant gain over the band matched energy detector.

The fact that the dynamical detector does not provide a performance gain over the energy detector for the 4000 RPM recording, can be explained by the fact that the signal amplitude was greater than the range of the ADC at a few samples during the recording. This degrades the performance of the dynamical detector drastically, while the band matched energy detector is hardly effected.

In the case of the hybrid detector we found similar gains as for the dynamical detector over all the data sets. In no case did the hybrid detector do worse than the energy detector or the dynamical detector. The hybrid detector did provide better performance on the 4000 RPM case.

In summary, even the simplest detector using a dynamical model utilized here appears to be more flexible and robust than standard band-matched energy methods. The principal result in this paper is thus that the dynamical modeling approach is viable on real-world data applications.

References

[1] Kadtke J.B., Péntek Á., *Automated signal classification using dynamical signal models and generalized higher-order data correlations (U)*, USN Journal of Underwater Acoustics, 2000.

[2] Lennartsson R.K., *Classification with dynamical models estimated with higher order statistical moments*, FOA Report, FOA-R-99-01292-313–SE, Defence Research Establishment, Sweden, 1999.

[3] Péntek Á., Kadtke J.B., *Detection of low-SNR signals using dynamical models estimated with higher-order data moments*, in Proceedings of the 1999 ASME Design Engineering Technical Conferences, September 12-15, 1999, Las Vegas, Nevada, USA, **DETC99/VIB-8366** (1999).

[4] Boashash B., Edward J.P., Abdelhak, M.Z., eds., *Higher-order statistical signal processing*, Longman and Wiley Press, Melbourne, 1995.

[5] Krzanowski W.J., and Marriott F.H.C., *Multivariate Analysis, Part 1, Distributions, Ordination and Inference*, Arnold, 1994.

[6] Anderson J.A., *Logistic Discrimination*, in Handbook of Statistics, Vol. 2, eds. Krishaiah, P.R., and Kanal, L.N., North-Holland, pp. 169-191, 1982.

[7] Krzanowski W.J., *A comparison between the distance-based discrimination principles*, Journal of Classification **4**, 73-84, 1987.

[8] Lennartsson R.K., Robinson J.W.C., Persson L., Hinich M.J. and McLaughlin S., *Passive sonar signature estimation using bispectral techniques,* Proceedings of the 10th IEEE workshop on Statistical Signal and Array Processing, SSAP 2000, Pocono, PA, USA, 2000.